All Sciences Proceedings

3rd International Conference on Innovative Academic Studies

September 26-28, 2023 : Konya, Turkey

ICIAS

All Sciences Proceedings
http://as-proceeding.com/

https://www.icias.net/

Structural Comparative Analysis of Nanocomposite Materials Comprising Mg, Zn, and Co Synthesized via Sono-electrochemical and Hydrothermal Approaches

Safia HARRAT [1, *], Mounir SAHLI [1], Khaled CHETEHOUNA [2]

[1]*Physics Department/Ceramics laboratory, Frère Mentouri Constantine 1 University, Algeria*
[2]*INSA Centre Val de Loir, PRISME laboratory EA 18000 Bourges, France*

** corresponding author: safia.harrat@student.umc.edu.dz*

Abstract – Nanocomposites based on magnesium (Mg), Zinc (Zn), and cobalt (Co) were synthesized using sonochemical and hydrothermal techniques. The structural properties of the nanocomposites were investigated. X-ray diffraction analysis revealed that the nanocomposites synthesized via the sonochemical method exhibited a complex crystalline structure comprising various crystalline phases: MgO, ZnO, Co_3O_4, and the binary phase Mg-Zn. In contrast, the nanocomposites obtained through the hydrothermal method showed only three phases: MgO, ZnO, and Co_3O_4. Furthermore, each exhibits distinct crystallite sizes. Scanning Electron Microscopy (SEM) was employed to examine the nanoparticle morphology, revealing octahedron-shaped nanoparticles with different average sizes for the nanocomposites obtained through the sonochemical method, while the hydrothermal method resulted in a mixture of rod and sheet morphologies with varying average sizes. Additionally, Fourier Transform Infrared Spectroscopy (FTIR) was utilized for sample characterization, revealing the presence of different functional groups in the nanocomposites.

Keywords – Sonochemical Synthesis, Hydrothermal Method, Morphology, Crystallite Phases, Nanocomposites

1. Introduction

The synthesis of nanocomposites within the field of nanotechnology has attracted considerable interest due to their potential value in a variety of applications such as gas sensors [1], supercapacitor application [2], photocatalytic activities [3], and hydrogen storage application [4]. The properties of their constituent materials are determined not only by the properties of their constituent parts but also by their structural structure and the way they interact with each other. As a result, nanocomposites promise to open up new applications in a wide range of files, including the reinforcement of mechanically robust lightweight components, the manipulation on nano-linear optical properties, the enhancement of battery cathodes, the fabrication of

advanced sensors, and other complex systems [1-5-6]. In the field of materials nanocomposites synthesis and advanced research, the choice of fabrication process is critical in defining the final properties and uses of synthesized materials. Sonochemical and hydrothermal processes have emerged in recent decades as prominent approaches to the synthesis of various materials due to their unique ability to control morphology, crystallinity, and other physicochemical [4-7]. Ultrasound is used in the sonochemical process to induce large pressure fluctuations in liquids. Bubbles form and collapse rapidly, creating high temperatures and pressures at microscale hotspots. This generates reactive species and accelerates chemical processes [8]. In addition, the hydrothermal approach involves the properties of water by using high temperature and pressures. In sealed vessels, it dissolves and interacts with materials. The altered conditions allow novel reactions and the controlled precipitation of nanoparticles or crystals [9].

The main objective of this research is to synthesize nanocomposites based on Mg, Zn, and Co using simple, rapid sonochemical and hydrothermal methods. Also, to compare the physical properties of samples prepared by these two different techniques and to elucidate the influence of the synthesis modality on the resulting phases, particle size, and morphological properties.

2. Experimental

2.1. Synthesis Methods

2.1.1. Sonochemical method

In one pot, a mixture of the three chemical precursors: magnesium chloride hexahydrate ((MgCl2).6H2O), zinc chloride (ZnCl2), and cobalt (II) chloride hexahydrate ((CoCl2).6H2O) was dissolved in deionized water with a molarity ratio of 1:1:1. The mixture is then stirred for 30 minutes with a magnetic stirrer at a temperature of 60 °C. The solution is sonicated for 15 minutes at a frequency of 20 KHz and an acoustic power of 1500 W to finish the reaction mechanism and guarantee high mixture homogeneity. After that, the mixture is dried for 48 hours at a temperature of 110 °C, turn it into powder and get rid of the water molecules. The dried powder is then calcined for a final 2 hours at 550 °C in a muffle furnace to form the Mg-Zn-Co nanoparticles. The synthesis method is summarized in Figure 1.

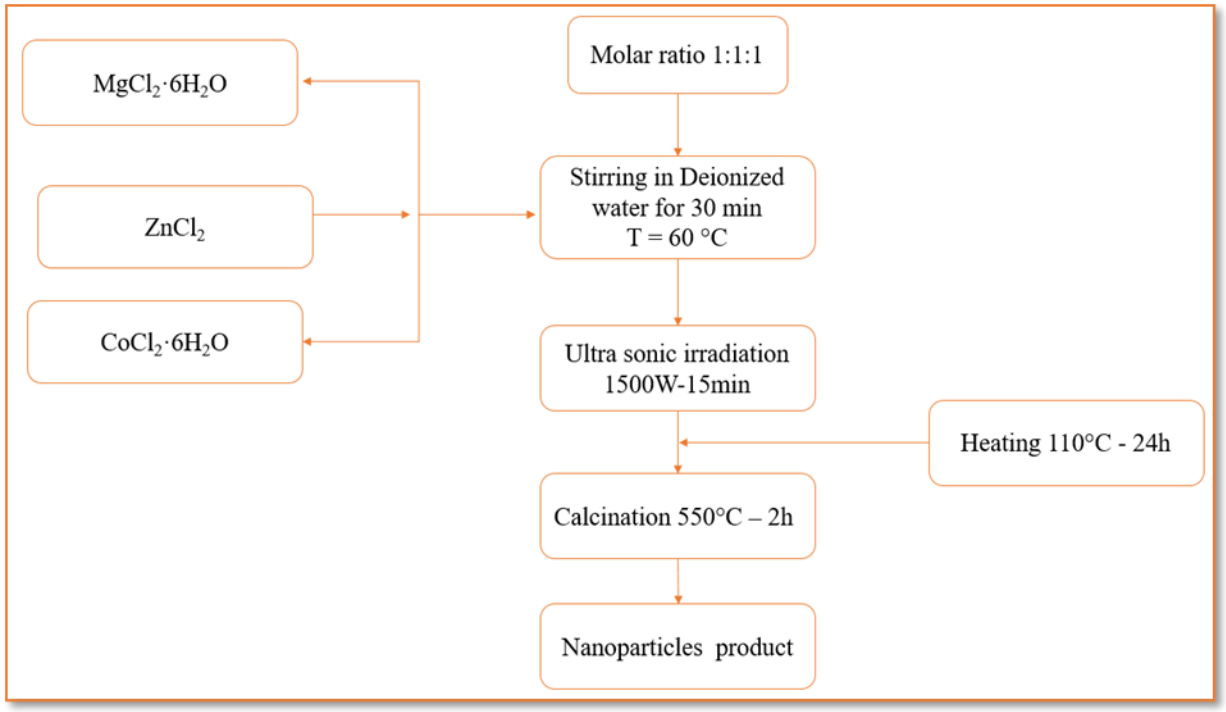

Fig. 1. Process diagram for Mg-Zn-Co nanoparticle synthesis by the sonochemical method (S1)

2.1.2 Hydrothermal method

The Mg-Zn-Co ternary nanocomposites were created in a single pot using the hydrothermal method. Starting materials include magnesium acetate tetrahydrate ($Mg(CH_3COO).4H_2O$), zinc acetate dihydrate ($Zn(CH_3COO)_2.2H_2O$), and cobalt acetate tetrahydrate ($2Co(CH_3COO).4H_2O$). These were mixed with deionized water, and Sodium hydroxide was used to bring the pH of the reaction up to 10. A Teflon-lined stainless steel autoclave was used to react the resulting mixture for 24 hours at 180 °C after stirring it for 30 minutes at room temperature. To create the desired Mg-Zn-Co nanocomposites powder, the resulting powder was cooled, washed with ethanol and deionized water, and dried at 60 °C for 12 hours to form Mg-Zn-Co nanoparticles. The synthesis method is summarized in Fig. 2.

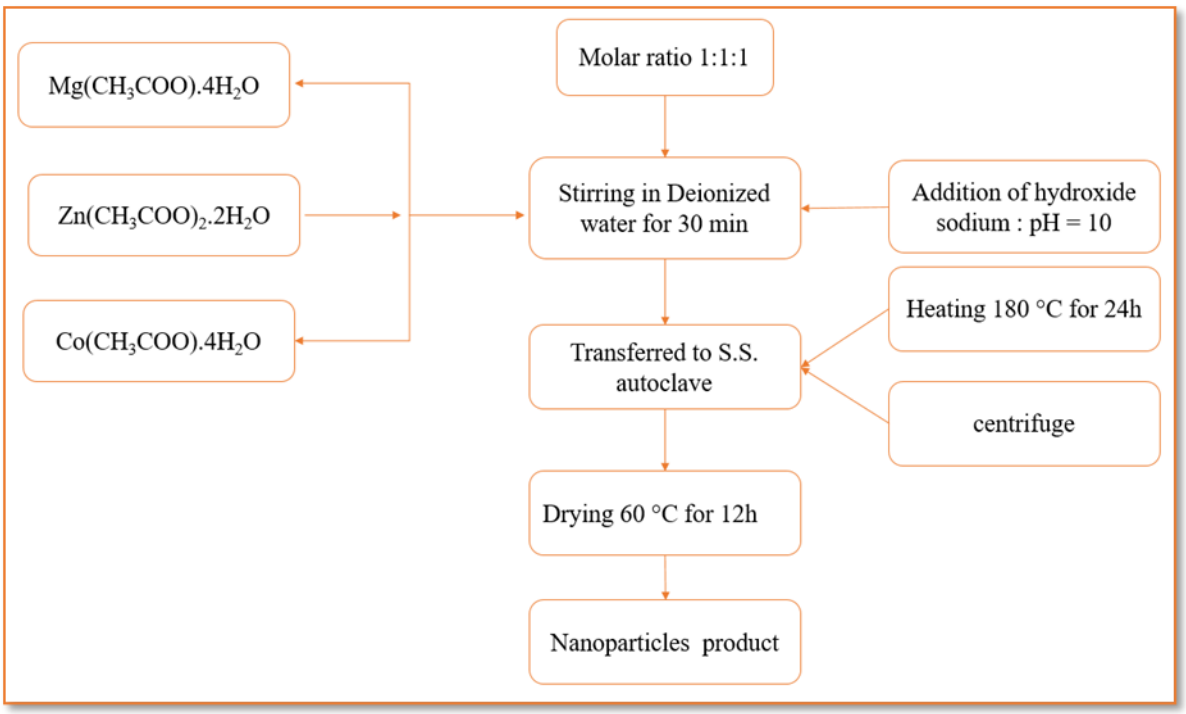

Fig. 2. Process diagram for Mg-Zn-Co nanoparticle synthesis by the hydrothermal method (S2)

2.2. Characterization methods

The structural characteristics of the samples were investigated using the following techniques: X-ray diffraction (XRD) analysis (XPERT-PRO diffractometer) was carried out to investigate the variation of valance and conduction bonds in the ternary samples. The analysis conditions were fixed at 45 KV and 40 Ma IN THE 2θ range of 10-80 cm^{-1} with CuKa radiation (1.5405 Å) and at a temperature of 25 °C. To complete the XRD analysis, the morphology of the investigated samples was studied using a scanning electron microscope (SEM, ZEISS Gemini 300, Germany). An energy dispersive spectrometer (EDS, ZEISS Gemini 300, Germany) was used for elemental analysis of the sample. A Jasco FT/130 IR-6300 instrument (Jasco Analytical Instruments, Easton, MD, USA) was used for FT-IR spectroscopy measurements to identify the functional group. The investigation was carried out in the frequency range of 400-4000 cm^{-1} with a resolution of 4 cm-1. The scan speed was 2 mm/S, and ATR technique was used with a TGS detector.

3. Results and discussion

3.1. XRD results

Figure 3 shows the spectra resulting from the XRD analysis of the samples. The data indicate the formation of three metal-oxide phases: magnesium oxide (MgO), zinc oxide (ZnO), and cobalt oxide (Co_3O_4) in the two samples. In addition, a second

metal-metal: Mg-Zn phase was observed, which was manifested during sample synthesis by the sonochemical method.

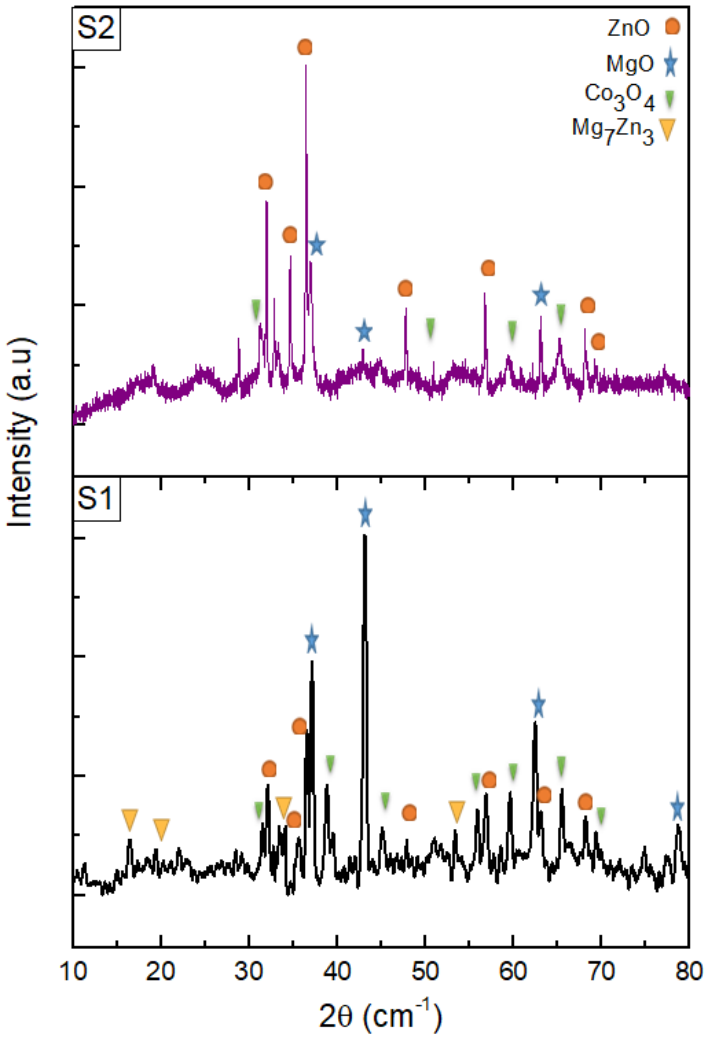

Fig. 3. XRD pattern for the investigated nanocomposite samples synthesized

The MgO phases were characterized by peaks at 2θ = 37.1°, 43.1°, 62.4°, and 78.75°, corresponding respectively to the (111), (200), (220), and (222) planes of a single-phase cubic system (JCPDS database card number 087-0653). The Co_3O_4 phase (cubic) was identified by peaks appearing at 2θ = 31.5°, 38.8°, 45.2°, 50.9° ,55.9°, 59.7°, 65.6°, and 69.35°, which were indexed to the (220), (222), (400), (331), (422), (511), (440), and (442) planes, respectively. (JCPDS database card number 74-1656). The XRD pattern also revealed the presence of ZnO nanocomposites belonging to the hexagonal

structure, characterized by peaks at 2θ = 32.1°, 34.7°, 36.5°, 47.7, 56.9°, 63.1°, 68.2°, and 69.3°, corresponding to the (100), (002), (101), (102), (110), (103), (112), and (201) planes, respectively. (JCPDS database card number 75-1565). Finally, the metal-metal phase, which was the Mg_7Zn_3 phase located at 2θ = 16.4°, 19.4°, 33.4°, 51.1°, and 53.3°, was indexed to the (220), (310), (332), (521), (800), and (653) planes, respectively. (JCPDS database card number 08-0269).

It should also be noted that the observed spectrum shows another difference in orientation between the sono prepared sample with MgO, marked by the dominant peak at (200) plan in the spectrum, and the hydrothermally prepared sample with ZnO, with a pronounced peak at (101) plan. These variations in peak positions indicate contrasting crystallographic orientations and crystalline structures between the two samples preparation methods.

The crystallite size of Mg-Zn-Co nanocomposites oxide was determined by using the Scherer equation (1) given below [10]:

$$D = \frac{K\lambda}{\beta COS\theta} \qquad (1)$$

Where D is the crystallite size, K is a dimensionless ship factor (0.9), λ is the X-ray wavelength (1.5406), θ is the Bragg angle, and β is the full width at half maximum intensity (FWHM).

Table. 1. Average crystallite size of the synthesized samples

Crystallite size	**Samples**	
	S1	**S2**
D (nm)	46.88	42.33

The determined crystallite sizes for the samples are presented in Table 1. It is observed that the crystallites obtained have nanoscale dimensions. However, a slight difference is observed in the crystallite size between the sample prepared through the hydrothermal method and that obtained through the sonochemical method. Specifically, the hydrothermal method yields slightly smaller crystallite sizes compared to the sonochemical method.

3.2 SEM analysis

Figure 4 shows the micrographs of the prepared samples, which show clear morphological differences. The sonochemically synthesized sample shows octahedral shapes and morphology of different sizes with all the phases mentioned above (XRD) [11-12-13]. This shape results from the coordination of the metal cations and oxygen anions. An octahedral structure consists of six oxygen atoms at the vertices, with a central metal

atom occupying the center [14]. When the pH of the starting solution is acidic [12]. This phenomenon is visible in our sample prepared by sonochemistry. The acidic pH was maintained without the inclusion of catalysts to facilitate its rise.

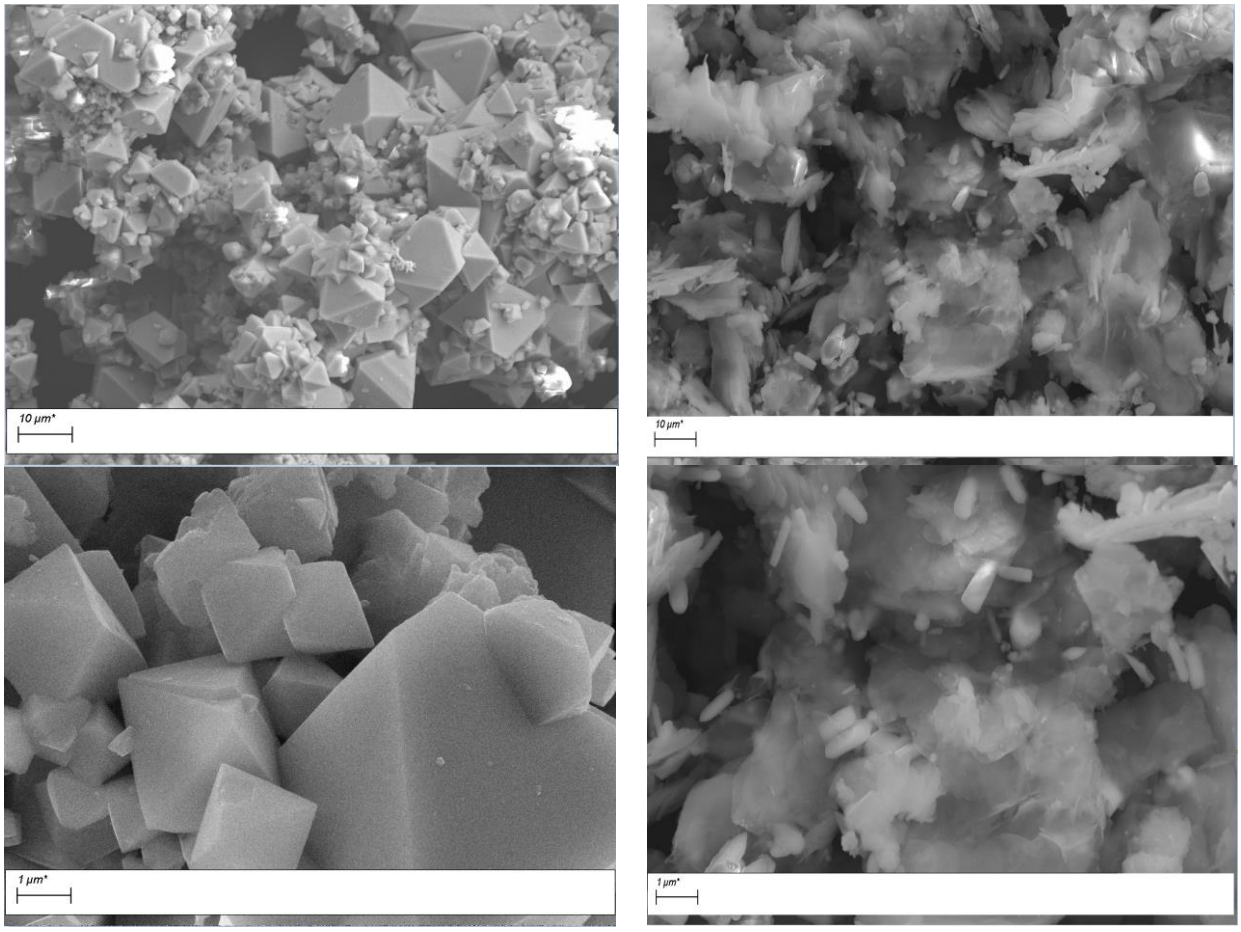

(S1) (S2)

Fig. 4. SEM micrographs of the studied nanocomposites

Conversely, the hydrothermally synthesized sample shows a combination of rod and sheet structures. Apparently, the rod structure corresponds to the hexagonal crystal structure of the ZnO phase [15]. While the sheet structures correspond to the Co3O4 and MgO phases [16-17].

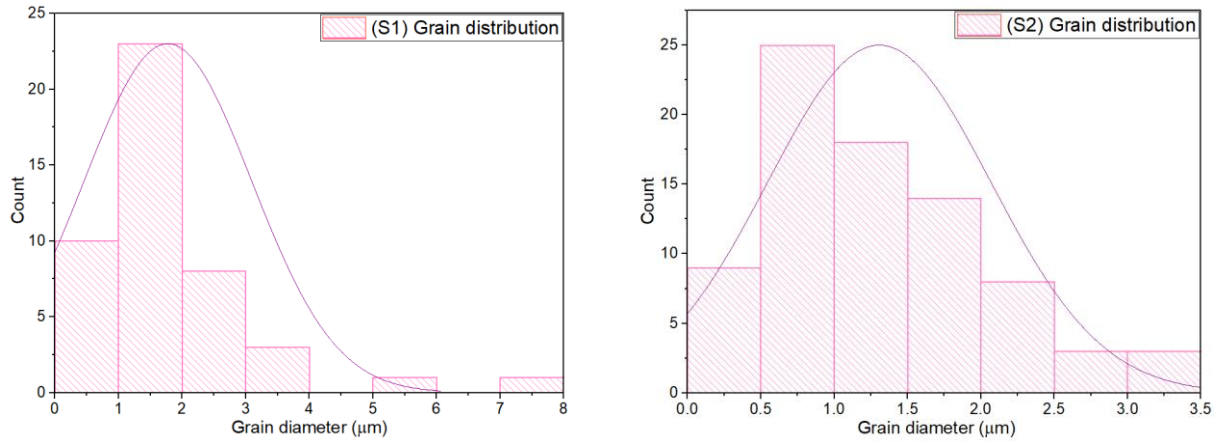

Fig. 5. Histogram representation of the grain distribution of the synthesized samples

The average grain size of the samples extracted from the histogram (Fig. 5) followed the same variation as the crystallite size (Table 1). The results indicate a slight difference in grain dimensions between the two samples.

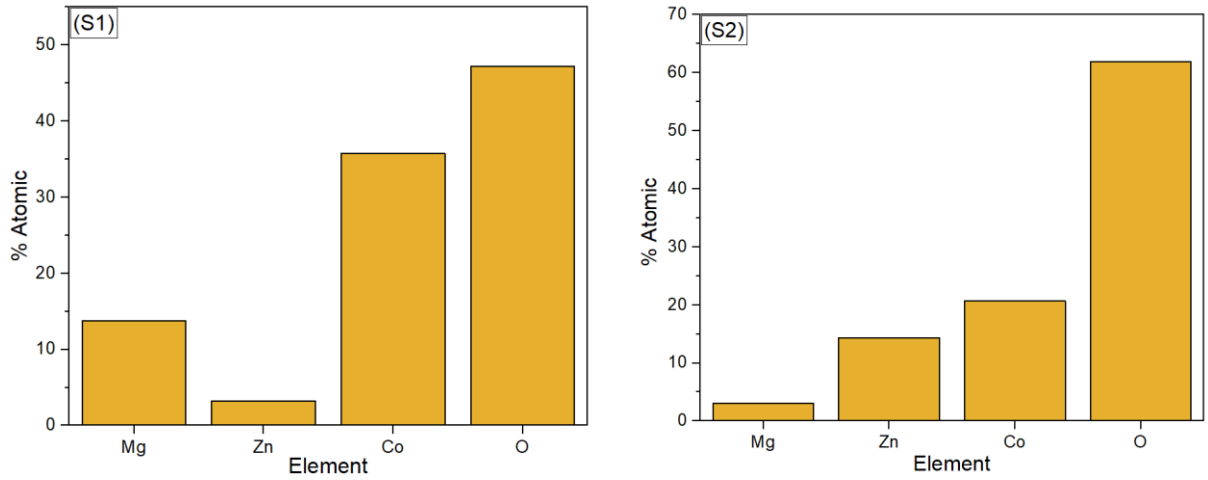

Fig. 6. EDC results for the synthesized samples

Figure 6 shows the EDS results of the samples analyzed, providing insight into the variations in the compositional rations of different compounds (Mg, Zn, Co, and O). Although an equal molar ratio (1:1:1) of these three atoms was used during sample preparation, significant differences are observed in

the relative percentages of Co and Mg, with their percentages being greater in the sonar-prepared sample than in the hydrothermal-prepared sample. The logical reason for this difference is that ultrasound had a more pronounced effect on the size and agglomeration of these materials. In contrast, the percentage of Zn shows an inverse trend.

It is also noteworthy that the proportion of Co has a higher affinity for diffusion compared to Mg and Zn in two samples. This discrepancy indicates that Co has a greater affinity for diffusion compared to Mg and Zn, suggesting a greater tendency to migrate within the samples.

3.3 FTIR Spectroscopy analysis

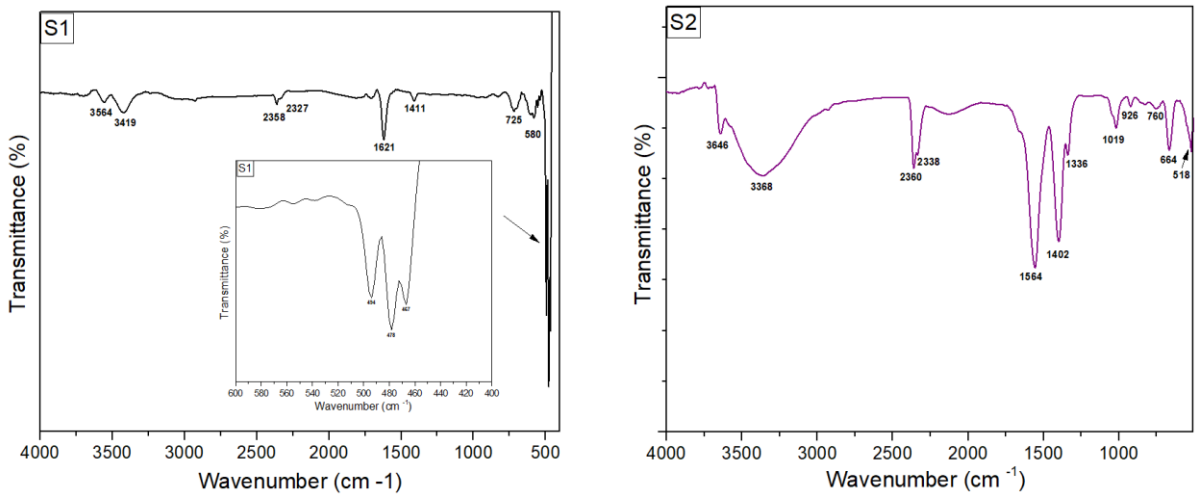

Fig. 7. FTIR spectrum for the synthesized samples

Figure 7 demonstrates the FTIR spectrum of nanocomposites prepared, with distinctive absorption bands indicative of common chemical constituents between the materials. The stretching and bending vibrations of the adsorbed water molecules are represented by spectral features centered on wave numbers 1620 cm^{-1} and 2330 – 2360 cm^{-1} [18]. Furthermore, the presence of carbon dioxide, can be linked to the observed peaks within the same wavenumber range at 2330 – 2360 cm^{-1} [19-20]. Within the 400-800 Cm^{-1} spectral region recognized for metal-oxygen (M-O) vibrations, unique peaks at 467 cm^{-1} , 494 cm^{-1}, and 580 cm^{-1} are detected as indicative of Zn-O, Mg-O and Co3+-O interactions, respectively [21-22-23], within the sonochemically prepared nanocomposites. Furthermore, significant peaks at 664 cm^{-1} , 760 cm^{-1}, and 926 cm^{-1} correspond to the Co2+-O, Mg-O and Zn-O vibrational modes, respectively [23-24-25].

Conclusion

The nanocomposites based on Mg, Zn, and Co were prepared by sonochemical and hydrothermal methods, and the nanocomposites obtained were characterized by structural methods. XRD diffraction confirms the formation of crystalline nanocomposite phases corresponding to MgO, ZnO, and Co3O4 in both simples, in addition to the Mg_7Zn_3 phase manifested in the sample prepared by the sonochemical method, with a convergence in crystallite size between the samples. SEM showed the octahedral shape of the surface, which was different from those obtained by the hydrothermal method, which showed a combination of rod and sheet structures. Finally, FTIR provided information on the functional groups and chemical bands present in the samples.

The results of this research show that the synthesis method plays a key role in determining the properties of nanocomposites. Factors such as stirring time, reaction temperature, calcination temperature, and pH were found to have a significant influence on the properties of the samples. This study provides valuable insights into tailoring the properties of nanocomposites by controlling the synthesis parameters and highlights the importance of selecting the appropriate method to achieve the desired properties in the final materials for each application.

References

[1] L. I. Trakhtenberg, G. N. Gerasimov, V. F. Gromov, T. V. Belysheva, and O. J. Ilegbusi, "Gas Semiconducting Sensors Based on Metal Oxide Nanocomposites," *JMSR*, vol. 1, no. 2, p. p56, Mar. 2012, doi: 10.5539/jmsr.v1n2p56.

[2] G. S. Kumar, S. A. Reddy, H. Maseed, and N. R. Reddy, "Facile hydrothermal synthesis of ternary CeO_2 –SnO_2 /rGO nanocomposite for supercapacitor application," *Funct. Mater. Lett.*, vol. 13, no. 02, p. 2051005, Feb. 2020, doi: 10.1142/S1793604720510054.

[3] P. Singh, P. Shandilya, P. Raizada, A. Sudhaik, A. Rahmani-Sani, and A. Hosseini-Bandegharaei, "Review on various strategies for enhancing photocatalytic activity of graphene based nanocomposites for water purification," *Arabian Journal of Chemistry*, vol. 13, no. 1, pp. 3498–3520, Jan. 2020, doi: 10.1016/j.arabjc.2018.12.001.

[4] N. A. Ali, N. H. Idris, M. F. M. Din, M. S. Yahya, and M. Ismail, "Nanoflakes MgNiO2 synthesised via a simple hydrothermal method and its catalytic roles on the hydrogen sorption performance of MgH2," *Journal of Alloys and Compounds*, vol. 796, pp. 279–286, Aug. 2019, doi: 10.1016/j.jallcom.2019.05.048.

[5] R. Kurahatti, A. Surendranathan, S. Kori, N. Singh, A. Kumar, and S. Srivastava, "Defence Applications of Polymer Nanocomposites," *DSJ*, vol. 60, no. 5, pp. 551–563, Jul. 2010, doi: 10.14429/dsj.60.578.

[6] H. Gao, W. Cai, P. Shimpi, H.-J. Lin, and P.-X. Gao, "(La,Sr)CoO3/ZnO nanofilm–nanorod diode arrays for photo-responsive moisture and humidity detection," *J. Phys. D: Appl. Phys.*, vol. 43, no. 27, p. 272002, Jun. 2010, doi: 10.1088/0022-3727/43/27/272002.

[7] A. E. Kandjani, M. F. Tabriz, and B. Pourabbas, "Sonochemical synthesis of ZnO nanoparticles: The effect of temperature and sonication power," *Materials*

Research Bulletin, vol. 43, no. 3, pp. 645–654, Mar. 2008, doi: 10.1016/j.materresbull.2007.04.005.

[8] H. Michael. Cheung and Shreekumar. Kurup, "Sonochemical Destruction of CFC 11 and CFC 113 in Dilute Aqueous Solution," *Environ. Sci. Technol.*, vol. 28, no. 9, pp. 1619–1622, Sep. 1994, doi: 10.1021/es00058a014.

[9] A. Nandagudi *et al.*, "Hydrothermal synthesis of transition metal oxides, transition metal oxide/carbonaceous material nanocomposites for supercapacitor applications," *Materials Today Sustainability*, vol. 19, p. 100214, Nov. 2022, doi: 10.1016/j.mtsust.2022.100214.

[10] S. Fatimah, R. Ragadhita, D. F. A. Husaeni, and A. B. D. Nandiyanto, "How to Calculate Crystallite Size from X-Ray Diffraction (XRD) using Scherrer Method," *ASEAN J. Sci. Eng.*, vol. 2, no. 1, pp. 65–76, Jun. 2021, doi: 10.17509/ajse.v2i1.37647.

[11] S. S. Sainudeen, L. B. Asok, A. Varghese, A. S. Nair, and G. Krishnan, "Surfactant-driven direct synthesis of a hierarchical hollow MgO nanofiber–nanoparticle composite by electrospinning," *RSC Adv.*, vol. 7, no. 56, pp. 35160–35168, 2017, doi: 10.1039/C7RA05812H.

[12] X. Xiao *et al.*, "Facile Shape Control of Co_3O_4 and the Effect of the Crystal Plane on Electrochemical Performance," *Adv. Mater.*, vol. 24, no. 42, pp. 5762–5766, Nov. 2012, doi: 10.1002/adma.201202271.

[13] J. Buasakun, P. Srilaoong, R. Rattanakam, and T. Duangthongyou, "Synthesis of Heterostructure of ZnO@MOF-46(Zn) to Improve the Photocatalytic Performance in Methylene Blue Degradation," *Crystals*, vol. 11, no. 11, Art. no. 11, Nov. 2021, doi: 10.3390/cryst11111379.

[14] W. Zhang *et al.*, "Magnetic transformation of Zn-substituted Mg-Co ferrite nanoparticles: Hard magnetism → soft magnetism," *Journal of Magnetism and Magnetic Materials*, vol. 506, p. 166623, Jul. 2020, doi: 10.1016/j.jmmm.2020.166623.

[15] R. Zhang, P.-G. Yin, N. Wang, and L. Guo, "Photoluminescence and Raman scattering of ZnO nanorods," *Solid State Sciences*, vol. 11, no. 4, pp. 865–869, Apr. 2009, doi: 10.1016/j.solidstatesciences.2008.10.016.

[16] Z.-Y. Li, P. T. M. Bui, D.-H. Kwak, M. S. Akhtar, and O.-B. Yang, "Enhanced electrochemical activity of low temperature solution process synthesized Co3O4 nanoparticles for pseudo-supercapacitors applications," *Ceramics International*, vol. 42, no. 1, pp. 1879–1885, Jan. 2016, doi: 10.1016/j.ceramint.2015.09.155.

[17] Q. Tian *et al.*, "Highly effective antibacterial activity of lithium-doped magnesium oxide particles synthesized by the microwave-assisted hydrothermal route," *Powder Technology*, vol. 371, pp. 130–141, Jun. 2020, doi: 10.1016/j.powtec.2020.05.031.

[18] R. Packiaraj, P. Devendran, K. S. Venkatesh, S. Asath bahadur, A. Manikandan, and N. Nallamuthu, "Electrochemical Investigations of Magnetic Co3O4 Nanoparticles as an Active Electrode for Supercapacitor Applications," *J Supercond Nov Magn*, vol. 32, no. 8, pp. 2427–2436, Aug. 2019, doi: 10.1007/s10948-018-4963-6.

[19] S. Kumari, P. Thakur, S. Singh, and A. Thakur, "A detailed structural analysis, morphological and optical study of Mg-Zn nano ferrite," *Materials Today: Proceedings*, vol. 73, pp. 233–236, 2023, doi: 10.1016/j.matpr.2022.07.201.

[20] M. Sahli, K. Chetehouna, F. Faubert, C. Bariki, N. Gascoin, and N. Bellel, "Experimental investigation on the concentration and voltage effects on the characteristics of deposited magnesium–lanthanum powder," *Appl. Phys. A*, vol. 119, no. 4, pp. 1327–1333, Jun. 2015, doi: 10.1007/s00339-015-9099-y.

[21] M. S, H. N, and V. P.P, "In Vitro Biocompatibility and Antimicrobial activities of Zinc Oxide Nanoparticles (ZnO NPs) Prepared by Chemical and Green Synthetic Route— A Comparative Study," *BioNanoSci.*, vol. 10,

no. 1, pp. 112–121, Mar. 2020, doi: 10.1007/s12668-019-00698-w.

[22] P. K. Singh, N. Singh, M. Singh, S. K. Singh, and P. Tandon, “Fabrication of nanostructured MgO and Zn-doped MgO as an efficient LPG sensing materials operable at room temperature,” *Appl. Phys. A*, vol. 127, no. 7, p. 563, Jul. 2021, doi: 10.1007/s00339-021-04712-5.

[23] A. Diallo, A. C. Beye, T. B. Doyle, E. Park, and M. Maaza, “Green synthesis of Co_3O_4 nanoparticles via *Aspalathus linearis*: Physical properties,” *Green Chemistry Letters and Reviews*, vol. 8, no. 3–4, pp. 30–36, Oct. 2015, doi: 10.1080/17518253.2015.1082646.

[24] M. R. Mohammad Shafiee, M. Kargar, and M. Ghashang, “Characterization and low-cost, green synthesis of Zn2+ doped MgO nanoparticles,” *Green Processing and Synthesis*, vol. 7, no. 3, pp. 248–254, Jun. 2018, doi: 10.1515/gps-2016-0219.

[25] M. S, H. N, and V. P.P, “In Vitro Biocompatibility and Antimicrobial activities of Zinc Oxide Nanoparticles (ZnO NPs) Prepared by Chemical and Green Synthetic Route— A Comparative Study,” *BioNanoSci.*, vol. 10, no. 1, pp. 112–121, Mar. 2020, doi: 10.1007/s12668-019-00698-w.